Desalination and Water Treatment
www.deswater.com
doi: 10.1080/19443994.2013.867411

53 (2015) 2565–2577
March

Taylor & Francis
Taylor & Francis Group

Treatment of arsenic (III) contaminated water by dynamically modified iron-coated sand (DMICS)

Deepa Srivastava, Rakesh Chandra Vaishya*

Department of Civil Engineering, Motilal Nehru National Institute of Technology, Allahabad 211004, India
Tel. +91 532 227 1315; Fax: +91 532 2545341; email: rcvaishya@yahoo.com

Received 18 May 2013; Accepted 1 November 2013

ABSTRACT

In this paper, dynamically modified iron-coated sand (DMICS) was synthesized by dynamic soaking of iron onto the sand. The DMICS was tested for As(III) removal from the aqueous solution by adsorption studies. The effects of particle size, initial arsenic concentration and adsorbent dose on arsenic removal efficiencies were evaluated by batch kinetic studies. Two batch kinetic models i.e. chemical reaction rate and pseudo-second order have been applied to see the behaviour of As(III) adsorption over DMICS. Langmuir, Freundlich and Temkin isotherms were used to describe the equilibrium studies data. Langmuir isotherm was found better fit when compared with other isotherms based on coefficient of correlation (R^2) values. The maximum adsorption capacity of DMICS was calculated as 0.29 mg/g as per Langmuir isotherm. The adsorption process was pH-dependent and maximum arsenic removal occurred in the pH range of 6–8. Scanning electron microscope was conducted on arsenic-loaded sand whereas, X-ray diffractogram (XRD) analysis was conducted on plain sand, DMICS and arsenic-loaded DMICS. XRD spectra supported the presence of arsenic on the surfaces of DMICS. The breakthrough and exhaustion times for 60 cm media column were 114 h and 200 h, respectively, based on column studies data. The DMICS has shown a good potential for arsenic remediation from aqueous medium.

Keywords: Arsenic adsorption; Dynamically modified iron-coated sand; Characterization; Batch kinetic models; Isotherms

1. Introduction

The presence of arsenic in groundwater and eventually in drinking water has been a serious environmental threat. It is hypothesized that arsenic is released to the environment mostly through natural processes, such as the presence of arsenical minerals, volcanic emissions and inputs from geothermal sources. Anthropogenic activities such as mining, combustion of fossil fuels and use of arsenical pesticides contribute arsenic in water [1,2]. Arsenic has been classified as a Class "A" carcinogenic compound as per US Environmental Protection Agency. Its presence has been reported in the groundwater of many countries like Argentina, Bangladesh, India, Pakistan, Mexico, Mongolia, etc. [3]. Based on human health risk assessment data, arsenic concentration of 10 μg/L in drinking water has been recommended by World Health Organisation as a guideline value [4]. In India,

*Corresponding author.

standard of 50 μg/L has been permitted in drinking water supplies as per BIS 10,500 [5].

Rural life is severely affected by arsenic problem at many places of third world countries, because groundwater is the only option for their drinking water source [6]. Acute arsenic poisoning includes stomach pain, nausea, vomiting or diarrhoea, which may lead to shock, coma and even death. Chronic arsenic poisoning may causes hypertension, peripheral vascular diseases, cardiac vascular diseases, respiratory diseases, diabetes mellitus and malignancies including cancer of the lungs, bladder, kidney, liver, uterus and skin [7]. As(III) is teratogenic and can damage the neurological system at aqueous concentrations of as low as 0.1 mg/L [8].

The bioavailability, toxicity and mobility of arsenic in the environment depend on its speciation [9]. Arsenic is most stable in As(III) and As(V) forms. Arsenite [As(III)] is converted to H_3AsO_3, $H_2AsO_3^{-1}$ and $HAsO_3^{-2}$ and Arsenate [As (V)] is converted to H_3AsO_4, $H_2AsO_4^{-1}$, $HAsO_4^{-2}$ and AsO_4^{-3} in aqueous medium at different pH. Arsenates are thermodynamically stable forms of inorganic arsenic, mostly dominant in surface water. Arsenite exists under reducing conditions in anaerobic underground water [10–12]. The arsenite is 25–60 times more toxic than the arsenate. The toxicity of arsenic decreases in the order of arsine > inorganic As(III) > organic As (III) > inorganic As(V) > organic As(V) > arsonium compounds and elemental As [13].

Nowadays, iron oxides and hydroxides such as hydrous ferric oxide, crystalline hydrous ferric oxide, goethite and akaganeite are becoming promising adsorbents for removing both As(III) and As(V) from water [14]. It is reported that iron-based adsorbents require fewer chemical pretreatments and have longer operational lives than ion exchange resins or activated alumina [15]. The various iron-coated sand filter media are being developed in the laboratory for treatment of arsenic from water. These media fall in the category of emerging technologies for arsenic 'removal [16,17].

Among the variety of adsorbents for arsenic removal, natural sand are promising because they are relatively cheap, readily available in different particle sizes and therefore, may easily be used as column filling in small-scale column plants. Various researches related to arsenic removal by iron oxide-coated sand are reported in the literatures [18,19]. Very few literatures are available where dynamic soaking of iron by sand was carried out before coating. The present paper reports batch and column studies on dynamically modified iron-coated mountainous river sand. During batch kinetic studies, effects of particle size, contact time and adsorbent dose were investigated. The batch results were modelled by two batch kinetic models. The equilibrium studies data were described by Langmuir, Freundlich and Temkin isotherms. Column studies were conducted at various depths of column to preliminary assessment of behaviour of media in fixed bed studies for the removal of arsenic.

2. Materials and methods

2.1. Materials

The iron salt "ferric nitrate" [$Fe(NO_3)_3{\cdot}9H_2O$ (Merck, India)] was used as main coating chemical. Stock arsenic solution (1000 mg/L) was prepared by the dissolution of sodium arsenite $NaAsO_2$ (John Baker, USA) in distilled water. Stock solutions were preserved using 1000 mg/L ascorbic acid [20]. The secondary standards were freshly prepared for each experiment from the stock solution using distilled water.

Quartz sand was collected from the bank of river Tons near Allahabad (India). The sand was washed with tap water to remove foreign impurities and dried later in sunlight followed by heating in an oven at 105°C. Dried sand was sieved for geometric mean sizes of 356, 460 and 768 μm by ASTM sieves. Before coating, sand was acid soaked in 1.0 M of HCl for 24 h and then rinsed with tap water and dried in an oven at 100°C for overnight. Dried sand was cooled off to room temperature and stored in capped PVC bottles.

2.3. Synthesis of DMICS

The media were synthesized by coating iron on sand surface by dynamically mixing sand with iron salt solution for 12 h on a rotatory shaker for more deposition of iron. A mixture was prepared by taking 200 g processed sand and then mixing it with 20 g of ferric nitrate [$Fe(NO_3)_3{\cdot}9H_2O$] and 150 ml of distilled water. The mixture was agitated on end-to-end shaker for 12 h and then it was placed in an oven at 110°C for 20 h on a glass tray (Borosil, India) to drive off all visible water. Thereafter, it was washed with distilled water until the washings were clear enough and subsequently it was again dried in an oven at 100°C for overnight. After drying, the media were reddish brown in colour and the developed media were capped in PVC bottles for storage and further use.

2.4. Characterization of DMICS

2.4.1. Iron content

The amount of Fe on the coated media were measured by aqua regia acid extraction technique by

soaking 1 g of coated media into 10 ml of aqua regia for 24 h as per Han et al. [21]. The suspension was filtered by Whatman No. 42 filter paper and total Fe concentration on media were measured using Atomic Adsorption Spectrophotometer (Model: Perkin Elmer, Analyst-200, USA).

2.4.2. XRD analyses

The mineralogical composition of DMICS was characterized and analysed by X-ray diffraction technique (XRD). X-ray diffraction patterns for identification of crystalline phases were collected on SIETRONICS XRD SCAN type diffractometer, operating with Ni-filtered CuKα radiation (λ = 1.541841 Å) by step scanning at 0.05 intervals in the range of 10°–100° at 2θ. The JCPDSWIN software (version 1997) was used for peaks identification.

2.4.3. Scanning electron microscopy (SEM)

The micro-structures and micro-morphology of the arsenic-loaded samples were observed by Field Emission Scanning Electron Microscope (FESEM) [Make Carl Zeiss NTS GmbH, Oberkochen (Germany), Model: SUPRA 40VP]. Prior to examination, the specimens' surface was sputtered with gold. The coating was applied using gold–palladium sputtering unit by generating Argon plasma, which is allowed to strike on the Au–Pd ring.

2.5. Batch adsorption kinetics

The batch sorption studies were carried out at room temperature ($30^{o} \pm 2^{o}$ C) on an end-to-end rotatory shaker at 38 ± 2 rpm. The reaction mixtures consisted a total volume of 100 mL As(III) solution in borosil glass BOD bottles containing initial arsenic concentrations 1.0 mg/L and coated media. A series of batch experiments were conducted for three sorbate concentrations i.e. 0.5, 1.0, 2.0 mg/L for kinetic uptake of As(III) by DMICS. The effect of contact time was studied with an initial arsenic concentration of 1.0 mg/L and adsorbent dose of 10 g/L. The pH was kept at 7.0 ± 0.1 and contact time was varied from 1.0 h to 8.0 h. The effect of dose of adsorbent was also studied by varying the dose from 5 to 15 g/L at a fixed pH of 7.0 ± 0.1 with an initial As(III) concentration of 1.0 mg/L and a contact time of 8 h.

2.6. Isothermal studies

To assess the impact of initial pH on arsenic uptake, experiments were performed by varying pH from 2 to 12 with an initial arsenic concentration of 1.0 mg/L and an adsorbent dose of 10 g/L at a fixed contact time of 8 h. The bottles were removed from shaker after desired contact time and supernatant was separated from adsorbent by "Whatman" No 42 (ashless) filter paper. The pH of each solution was measured before and after sorption experiments by pH meter (Thermo Orion, US). The adsorption isotherms were obtained at different pH and particle sizes to find out capacity of the media for arsenic removal. Isothermal studies were also conducted with varying initial As(III) concentrations from 0.5 to 3.5 mg/L with a fixed adsorbent dose of 10 g/L, and for a contact time of 8 h. The pH drift during experimental studies was also measured. Other experimental conditions were similar to the batch kinetic experiments.

2.7. Column study

The fixed bed experiments were carried out in a borosilicate glass column (23 mm internal diameter and 60 cm height), which act as fixed-bed down-flow reactors. The column was packed with 336 g of DMICS media (0.460 mm size). The packed bed was supported on 5.0 cm thick glass wool at bottom. The synthetic solution containing 1.0 mg/L of As(III) was used as feed water. The flow rate of 1.54 $m^3/m^2/h$ was maintained through the column using a peristaltic pump (Watson Marlow, Germany). Effluent samples were collected at regular intervals and were analysed for residual arsenic concentrations. Columns were also operated at different bed depths of 20, 40 and 60 cms.

2.8. Toxicity characteristic leaching procedure (TCLP) test

The TCLP test was applied to the As-loaded adsorbents used in the column experiments. The spent adsorbent was extracted with the extraction fluid i.e. 5.7 mL of glacial CH_3COOH added to 500 mL of distilled water, plus 64.3 mL of 1 N NaOH and diluted to 1 L. It was adsorbed with a liquid/solid ratio of 20. The extraction was achieved by shaking the mixture for 18 h in an orbital shaker. The supernatant was separated using Whatman No. 42 filter paper and analyzed for total Arsenic [22].

2.9. Analytical method for aqueous arsenic determination

The concentrations of As(III) in the laboratory samples were measured by Johnson & Pilson method using spectrophotometer (Model: Genesys-20, Thermo Spectronic, US) [23]. The detection limit of As(III) was 4 μg/L.

3. Results and discussion

3.1. Characteristics of the adsorbent

Inorganic composition of sand obtained from bank of river Tons near Allahabad, India was evaluated using X-ray fluorescence spectrometer (XRF) and is presented in Table 1. Table 2 shows amount of iron attached on the DMICS surface. Results show that the medium size of sand binds maximum amount of iron. Batch and column studies samples were tested to assess the impact of leaching of iron from modified coated sand and after each experiment, the filtered samples were tested for residual iron concentrations. The measured iron concentrations in all the samples were below the detection limit. This may suggest that the DMICS is a stable adsorbent for treating As(III) in aqueous medium.

3.1.1. X-ray diffractograms (XRD) studies

XRD of plain sand, DMICS and As(III)-loaded DMICS are given in the Fig. 1. Comparing the XRD data with the JCPDS file, the peaks of plain quartz sand were identified as the combination of silica oxide (SiO_2), aluminum oxide (Al_2O_3), iron silicate hydroxide hydrate [$Fe_2Si_2O_5(OH)_4{\cdot}2H_2O$] and $Ca_{12}Al_2Si_4(SO_4)_3F_{40}{\cdot}45H_2O$. The sharp peaks located on the 30.58° (PDF No. 15–0026) and 26.84° (PDF No. 33–1161) at 2θ can be attributed to SiO_2. Other sharp peak arising at 53.83° (PDF No. 26–1140) is an indicative of iron silicate hydroxide hydrate [$Fe_2Si_2O_5(OH)_4{\cdot}2H_2O$]. Peaks located at 31.54° and 29.6° at 2θ are revealing the presence of Al_2O_3 (PDF No. 46–1131). Some other faint peaks at 21.1°, 27.8°, and 29.6° at 2θ represent to $Ca_{12}Al_2Si_4(SO_4)_3F_{40}{\cdot}45H_2O$ (PDF No. 30–0228). Few minor/faint peaks at 22.3° and 27.8° at 2θ (PDF No. 45–0406) suspect the presence of Aluminum oxide silicate ($283SiO_2{\cdot}Al_2O_3$).

From the iron coating on the sand surface, goethite peaks dominate the patterns at 27.58°, 36.56° and 68.24° at 2θ indicating that the adsorbed Fe(III) decomposed to form FeOOH (PDF No. 44–1415). The mineralogy of the iron coated onto the DMICS depends on the temperature of coating. From the iron coating on silica, amorphous iron oxide forms at 60°C, goethite and hematite forms at 150°C and hematite above 300°C [24]. Three predominant peaks at 26.84° and 50.25° at 2θ (PDF No. 46–1045) confirm the presence of quartz on the DMICS. Various faint peaks at 39.50°, 67.75°, 60.05°, and 29.75° at 2θ (PDF No. 46–1131) reveal the presence of δAl_2O_3.

The XRD analysis of arsenic-loaded DMICS confirmed the existence of SiO_2 at 27.94° at 2θ (PDF No. 03–0276). The second largest peak at 27.49° at 2θ indicates to the FeOOH (PDF No. 44–1415). Various faint peaks present at 10.5°, 11.4°, 20.86°, 23.6°, and 25.15° at 2θ (PDF No. 28–0485) reveal the presence of iron hydrogen arsenate hydrate [$Fe(H_2AsO_4)_3{\cdot}5H_2O$]. Arsenic was adsorbed in a very little amount therefore peaks at 10.5°, 11.4°, 23.6°, and 25.15° at 2θ mixed in noise zone.

Table 1
Characterization of Tons river sand

Contents	% Composition
Na_2O	2.69
MgO	0.18
Al_2O_3	9.21
SiO_2	81.81
P_2O_5	0.01
K_2O	4.40
CaO	0.50
TiO_2	0.14
MnO	0.01
Fe_2O_3	0.78
SUM	99.73
LOI	0.89

Table 2
Fe concentration on the sand after coating

Sl. no.	Particle size (mm)	Fe (mg/g of sand)
1.	0.358	9.08
2.	0.460	15.12
3.	0.768	11.68

3.1.2. SEM studies

SEM photographs presented in Fig. 2 were taken at 100X, 2000X magnifications to observe the surface morphology of the As(III)-loaded DMICS. The typical surface of the As(III)-loaded DMICS particles as observed from SEM pictures was uneven and chapped like. Rough surface structure may be formed due to the presence of iron on the surface of DMICS. Extensive flow through exposure of arsenic during adsorption process may have smoothened the existing surface structure.

3.2. Influence of pH on adsorption capacity

The adsorption of As(III) onto DMICS at different pH values was studied to clarify the influence of solution pH on the adsorption capacity and to establish the optimum pH for the adsorption of arsenic in these

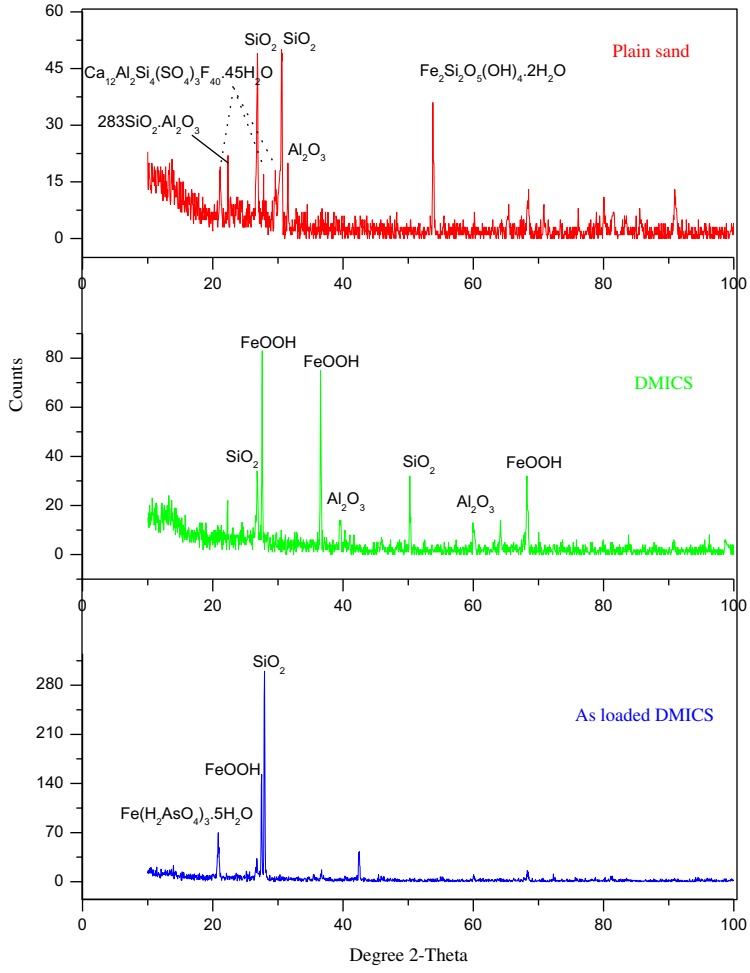

Fig. 1. XRD of plain sand, DMICS and As(III)-loaded DMICS.

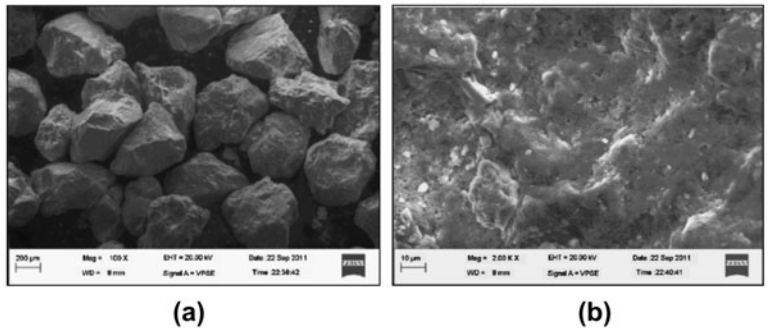

Fig. 2. SEM images of As(III)-loaded DMICS at different magnification (a) 100 X; (b) 2000 X.

pH ranges. Fig. 3 shows the adsorption capacity for the As(III) as a function of initial pH. It was found that arsenic removal by the DMICS was pH-dependent and the maximum removal took place at near-neutral pH (pH range of 6.5–7.5). The removal was found to increase with the increase in pH range from 2 to 7.5 and decreased with the further increase in pH. Wilkie and Hering also observed similar patterns of arsenic immobilization near neutral pH in their studies [25]. The percentage arsenic adsorption was greater than 90% throughout the pH range of 4–7. The As(III) adsorption was clearly less dependent on the pH in

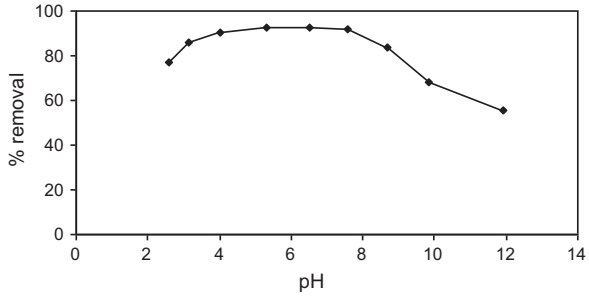

Fig. 3. Effect of pH on As(III) percentage removal.

the range of 3–8, and reached broad maxima from approximately pH 6.5 to 7.5. The adsorption of neutral H_3AsO_3, which is the dominant As(III) species at a wide pH range of 2–9, would be less strongly influenced by the anion repulsion forces that would likely play an important role in the adsorption of As(III) species at high pH. Singh et al. have also observed the maximum adsorption of As(III) on a hematite ore at pH 7 [26]. Zeng found the maximum adsorption of As (III) from pH 6.5 to 8.6 [27].

The measured pH_{ZPC} of DMICS was 7.3 (Figure not shown here). Thus below this pH, the surface of adsorbent acquires positive charge; and above this pH, it is negatively charged. The neutral H_3AsO_3 is a prominent species up to pH 9.2 but slight dissociation of H_3AsO_3 may start from pH 7.0 onwards. As the pH increases, the number of negative arsenic species increases, while the number of positive charge surfaces will also decrease. This hypothesized the decrease of As(III) removal at higher pH.

3.3. Adsorption equilibrium

The experimental adsorption equilibrium data for As(III) was modelled using the various isotherms showed in Table 3. Adsorption isotherms of As(III) onto DMICS are shown in Figs. 4–6. The parameters values of Langmuir, Freundlich and Temkin isotherms

Table 3
Equation of isotherm models for adsorption equilibrium

Isotherms	Equations	References
Langmuir	$q_e = \frac{Q_0 b C_e}{1 + b C_e}$	[28]
Freundlich	$q_e = K_F C_e^{1/n}$	[13]
Temkin	$q_e = A + B \ln C_e$	[29]

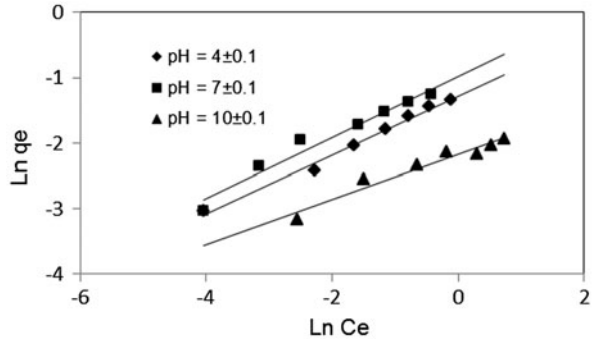

Fig. 4. Freundlich model curves for As(III) adsorption at different pH.

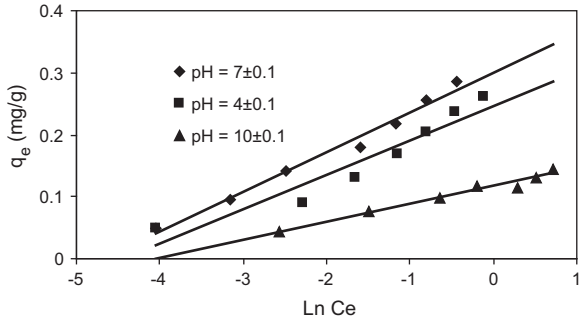

Fig. 5. Temkin isotherms for As(III) adsorption at different pH.

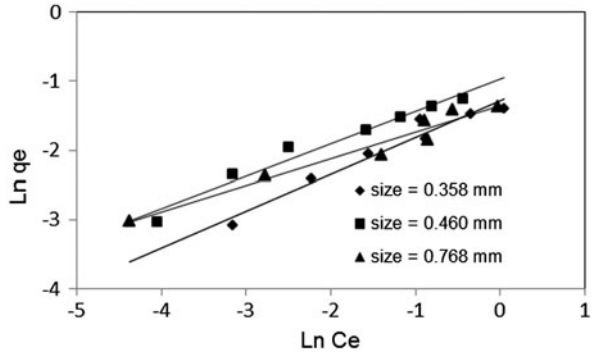

Fig. 6. Freundlich model plots for As(III) adsorption at different media size.

are presented in Table 4. Based on R^2 values, Langmuir isotherm is better fitted with the experimental data when compared with other two isotherms. However, the total arsenic removal can also be described by the both Freundlich and Temkin isotherms. A slightly lower R^2 values were obtained for these two isotherms than those of the Langmuir isotherm. Generally, the applicability of the two parameters

Table 4
Parameters for As(III) adsorption on DMICS for different isotherms

Variables		Langmuir constants			Freundlich constants			Temkin constants			
pH	Size (mm)	Q_0 (mg/g)	b (L/g)	R^2	K_F (mg/g)	1/n	R^2	B (mg/g)	A (L/g)	R^2	pH drift
4 ± 0.1	0.460	0.20	18.02	0.92	0.28	0.45	0.99	0.056	83.09	0.91	5.97–6.17
7 ± 0.1	0.460	0.29	11.49	0.99	0.38	0.47	0.97	0.064	108.13	0.98	6.09–7.21
10 ± 0.1	0.460	0.14	5.56	0.99	0.11	0.34	0.95	0.029	60.21	0.97	9.13–10.15
7 ± 0.1	0.357	0.28	5.24	0.99	0.28	0.53	0.95	0.065	41.19	0.94	7.06–7.23
7 ± 0.1	0.768	0.19	27.03	0.92	0.26	0.38	0.95	0.047	148.41	0.84	6.84–7.29

isotherm models approximately follows the order: Langmuir > Freundlich > Temkin. The fitting of Langmuir isotherm does not indicate that only sorption phenomenon has taken place [30].

Changes in the sorption capacities were observed along with the changes in pH (Figs. 4 and 5) and media size (Fig. 6). The reason for these trends may be due to different species distribution of As(III) in aqueous medium at various pH. The adsorption dependence on three different isotherms may be explained partially by assuming that oxide surfaces have different types of surface sites, with different affinities for adsorbate ions. The surface density for strong binding sites would be much less than the weaker binding sites. So, adsorption proceeds until all the strong binding sites are occupied, which will follow the Langmuir isotherm. Thereafter, the sorbate would start to adsorb on the weaker binding sites and if they are large in numbers then, pattern of isotherm will follow Freundlich isotherm. The Langmuir model is better fit to the data than Freundlich and Temkin models. The high values of "b" indicate the steep initial slopes of sorption isotherm which shows the high affinity for media. It also indicates the high adsorption energy and relatively faster increase in adsorption at low concentration of adsorbate [31].

The isotherms discussed above clearly exhibit non-linear and favourable behaviour. The non-linear or concentration-dependent adsorption behaviour was characterized by the low values of the Freundlich parameter 1/n, i.e. much less than 1 (Table 4). Low 1/n values for arsenic adsorption have been reported by other researchers also [32]. The 1/n is a measure of the extent of heterogeneity of the sorption sites having different affinities for solute retention by sorbent surfaces. In addition, 1/n illustrates the dependence of the sorption process on pH where sorption by the highest energy sites takes place preferentially at the neutral pH.

The post pH was measured after the each experiment. At initial pH 4 ± 0.1, the observed post pH ranged from 5.97 to 6.17. At initial pH 7 ± 0.1, the observed post pH ranged from 6.09 to 7.21, whereas in case of pH 10 ± 0.1, the post pH varied from 9.13 to 10.15 (Table 4). It was found that dissociation of sorbent particles in the process of shaking in rotatory shaker; ferric hydroxide may have been released into the aqueous medium. The addition of ferric hydroxide during experiment may have some "buffering effect". The resultant observed post pH was around the neutral pH except at pH 10 ± 0.1, where buffering effect was not so dominant. The "'buffering"' effect can be explained by the amphoteric nature of the iron oxide as given in Eqs. (1) and (2) (≡ donates surface group) [33].

$$\equiv \mathrm{FeOH}^{2+} = \equiv \mathrm{FeOH} + \mathrm{H}^{+} \quad (1)$$

$$\equiv \mathrm{FeOH} = \equiv \mathrm{FeO}^{-} + \mathrm{H}^{+} \quad (2)$$

At low pH medium, the equilibrium of Eqs. (1) and (2) shift towards left, resulting in an increase in the bulk solution pH. In a high pH medium, the acid dissociation dominates which may cause a decrease in the bulk solution pH [27].

Several researchers have used iron-based adsorbents for arsenic removal in past. Table 5 shows adsorption capacities (mg/g) of various adsorbents based on Langmuir & Freundlich isotherms. The present capacity of DMICS can be compared with referenced studies [34–38] as mentioned in Table 5. In comparison to other studies DMICS has shown relatively higher As(III) removal capacity.

Consequently, the equilibrium arsenic-removal coefficient b can be used to calculate a dimensionless constant separation factor or equilibrium parameter K_s, which is considered as a more reliable indicator of ion removal process in batch systems [39].

This parameter is defined by the following relationship:

$$K_s = \frac{1}{1 + bC_0} \quad (3)$$

Table 5
Uptake of As(III) onto some reported media along with DMICS

Adsorbents	Isotherms	Capacity (mg/g)	References
Iron oxide coated sand	Langmuir	0.028	34
Iron oxide coated sand	Langmuir	0.041	21
Sulfate-modified iron	Langmuir	0.140	35
Activated alumina	Freundlich	0.220	36
Iron oxide coated sand	Langmuir	0.136	37
laterite soil	Langmuir	0.180	38
DMICS	Langmuir	0.290	Present study

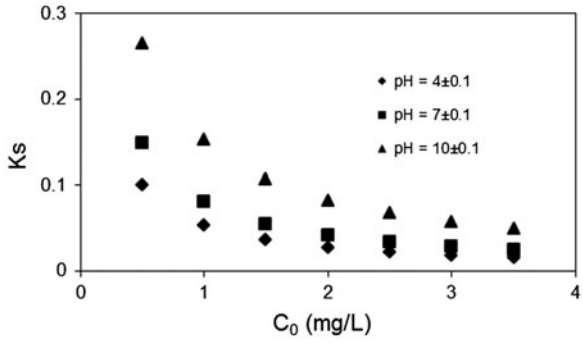

Fig. 7. Dimensionless constant separation factor at different pH.

where b = parameter of Langmuir equation, (L/mg) a constant related to energy and enthalpy of the system; C_0 = initial As(III) concentration in the aqueous phase, (mg/L).

For favourable removal process, $0 < K_s < 1$; while $K_s > 1$ represents unfavourable removal process, and $K_s = 1$ indicates linear removal process. If $K_s = 0$, the removal process is irreversible. For the concentration range considered in this study, the removal process of As(III) is favourable as K_s values lies between 0 and 1 (Fig. 7).

3.4. Adsorption kinetics

3.4.1. Effects of particle sizes, adsorbent dose and initial concentration

The rate of adsorption of As(III) was fast in the initial stages of the process, but it gradually decreased approaching equilibrium (Fig. 8). As expected, the time to reach equilibrium increased with increasing initial metallic ion concentration in the solution. In the first hour of mixing, approximately 75% of arsenic was adsorbed on the DMICS surface. The removal was then almost stabilized after 6h implying that the equilibrium has been reached. However, 8h equilibrium time was selected for all the experiments for being on safer side.

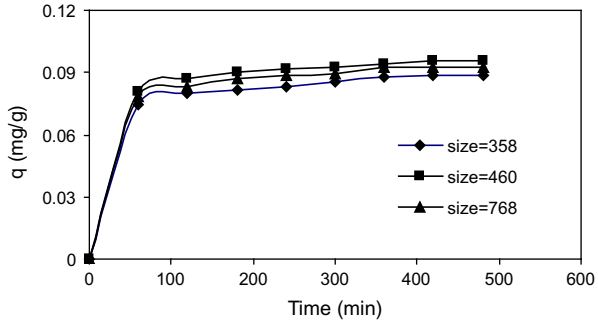

Fig. 8. Effect on particle size on As(III) removal by DMICS.

Fig. 8 shows that the medium size particles (i.e. 0.460 mm) have shown better removal capacity when compared with other two sizes. This may be due to the better coating of medium size sand particles than the other sizes. The higher Fe concentration on media surface may be a reason for higher As(III) removal when compared with the larger size particles (Table 2). Under the present experimental conditions, the effect of particle size has a slight influence on the adsorption rate.

Fig. 9 shows that q decreases with the increase in sorbent dose. An increase in the adsorption with the increase in adsorbent dosage can be attributed to availability of greater surface area and more adsorption sites. Arsenic adsorption at a dose of 10 g/L was measured about 94 percent; therefore, it was selected as optimum dose for further batch kinetic and isothermal studies. Observed post pH of the solutions was

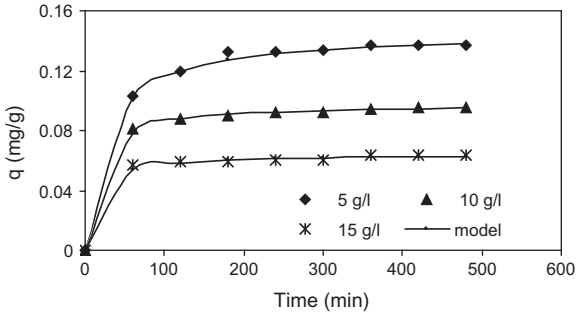

Fig. 9. Fitting of reaction rate model for As(III) adsorption onto DMICS at different adsorbent doses.

found to be independent of adsorbent doses. It can be seen from the Table 5, that the variation in adsorbent doses has little effect on pH drift and observed post pH shuttled from 6.70 to 7.03.

3.5 Kinetic models

The adsorption kinetics also depend on the interactions between adsorbent and As(III) ion concentrations, as well as on the system conditions, so to identify the rate-controlling mechanisms during the adsorption of arsenic, three main steps were considered: (1) mass transfer of the As(III) ions from the bulk solution to the DMICS surface, (2) adsorption of the As(III) ions onto sites and (3) internal diffusion of the As(III) ions onto DMICS. For this purpose, two simplified models were applied to evaluate the experimental batch data: chemical reaction rate model and pseudo-second-order model.

The rate constant of adsorption was determined from the reaction rate model. This model is based on mass law concept [11]. The adsorption kinetics on oxide-coated sand may be treated as a chemical reaction. This equation may be represented by a second-order reaction of the form:

$$M + S \xrightarrow{K_R} (MS) \tag{4}$$

where M represents the dissolved metal contaminant; S, the available surface sites; MS, the adsorbed state; and K_R, the reaction rate constant (L/mg·h). The rate equation is expressed in terms of concentrations of respective reactants. The rate constant K_R may be determined by least square linear regression of ln $[(C-C_e)/C]$ vs. t. The slope of the line provides a value of $-K_R$. The linear form of this equation is given below:

$$\ln\left(\frac{C - C_e}{C}\right) = -C_e K_R t + \ln\left(\frac{C_0 - C_e}{C_0}\right) \tag{5}$$

where C = liquid-phase As(III) concentration at time t, (mg/L); C_e = liquid-phase As(III) concentration at equilibrium, (mg/L); t = time (h); The plot of ln $[(C - C_e)/C]$ vs. t will give a straight line with slope of $-C_eK_R$ and intercept of $[(C_0 - C_e)/C_0]$.

The pseudo-second-order model is based on the assumption that sorption capacity is proportional to the number of active sites occupied on the sorbent and the rate-limiting step may be chemical sorption or chemisorption involving valancy forces through sharing or exchange of electrons between sorbent and sorbate. It provides the best correlation of the data; whereby the rate of sorption is proportional to the square of the number of unoccupied sites:

$$dq/dt = K_2(q_e - q)^2 \tag{6}$$

where q = amount of As(III) adsorbed at time t, (mg/g); q_e = amount of As(III) adsorbed at equilibrium, (mg/g); t = time, (min); K_2 = rate constant of pseudo-second-order adsorption, (mg/g·min).

Integrating Eq. (6) from $t = 0$ to $t = t$ and $q = 0$ to $q = q$ and linearization yields:

$$t/q = 1/(K_2 q_e^2) + t/q_e \tag{7}$$

The plot of (t/q) vs. t of Eq. (7) should give a linear relationship from which q_e and K_2 can be determined from the slope and intercept of the plot, respectively.

Statistical criteria used for estimating the goodness-of-fit of the models to the data were the coefficients of co-relation (R^2) and the root-mean-square error (RMSE).

$$\text{RMSE} = \sqrt{\frac{\sum (q_{exp} - q_{mod})^2}{N - 1}} \tag{8}$$

where q_{exp} = experimental value of As(III) adsorbed at certain time t, (mg/g); q_{mod} = model-simulated value of As(III) adsorbed at time t, (mg/g); N = number of measurements.

The model parameters and RMSE values for both the models are presented in Table 6. The values of kinetic parameters are substituted in the model equations to calculate sorption capacity (q) at various times by both the models.

Fig. 9 shows fitting of reaction rate model for As (III) adsorption onto DMICS at different adsorbent doses. Fig. 10 shows effect of sorbent dose on pseudo-second-order reaction rate constant. According to the pseudo-second-order model, the values of q_e decreases with the increase in dose from 5 to 15 g/L whereas, with the increase in dose, second-order reaction rate constant (K_2) also increased. It may be due to increase in rate of reaction with the increase in dose. The linear relationship was lacking in the reaction rate model at higher doses. Although both the models gave a good fit for all the three sorbent doses. This trend supports the pseudo-second-order sorption capacity which is proportional to the number of active sites occupied on the sorbent. These values suggest that the values of q_e increased for the lower doses of media at any specific

Table 6
Parameters of kinetic models for removal of As(III) by DMICS

Parameters		Pseudo-second order model				Reaction rate model			
C_0 (mg/L)	m (g/L)	K_2 (g/mg·min)	q_e (mg/g)	R^2	RMSE (%)	K_R (L/mg·h)	R^2	RMSE (%)	pH drift
0.5	10	0.68	0.050	0.997	0.16	8.38	0.74	0.63	7.42–7.60
1.0	10	0.67	0.098	0.999	0.12	3.88	0.96	0.10	6.77–6.95
2.0	10	0.51	0.170	0.999	0.27	0.82	0.91	0.19	7.27–7.52
1.0	05	0.29	0.145	0.999	0.21	1.69	0.87	0.31	6.83–7.03
1.0	15	1.40	0.064	0.997	0.16	1.40	0.93	0.19	6.70–6.88

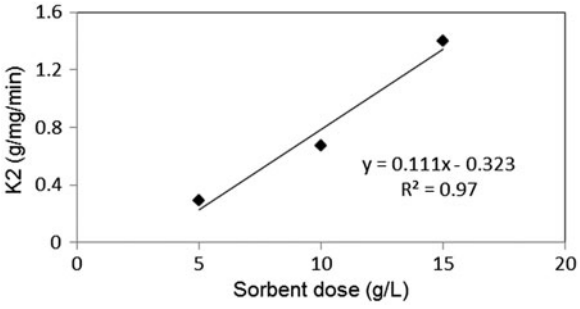

Fig. 10. Effect of adsorbent dose on pseudo-second-order reaction rate constant.

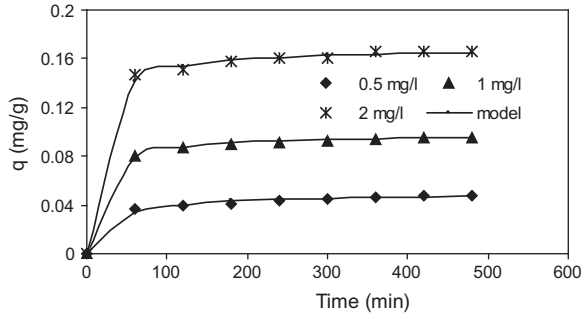

Fig. 11. Fitting of pseudo-second-order model for As(III) adsorption onto DMICS at different initial As(III) concentrations.

time (Table 6). The linear plot between K_2 and m has a good correlation with correlation coefficient value as 0.97 and is shown in the Eq. (9):

$$K_2 = 0.11\mathrm{m} - 0.32(R^2 = 0.97) \quad (9)$$

where m = dose of DMICS (g/L).

The values of qe and K_R were found to decrease with the increase in the initial concentration from 0.5 to 2.0 mg/L. It may be due to the availability of fewer active sites for sorption/reaction. The plots of kinetic models and experimental data are displayed in Figs. 11 and 12, which shows that the experimental concentration data are well fitted to the above-mentioned models. The following relationships were obtained between mass transfer rates and initial As(III) concentrations:

$$K_R = -4.281C_0 + 9.07(R^2 = 0.94) \quad (10)$$

$$K_2 = -0.12C_0 + 0.76(R^2 = 0.92) \quad (11)$$

The pseudo-second-order model shows the good correlation in overall study, therefore the rate controlling mechanism may be chemisorption (reaction rate). Based on coefficient of correlation (R^2) value, the

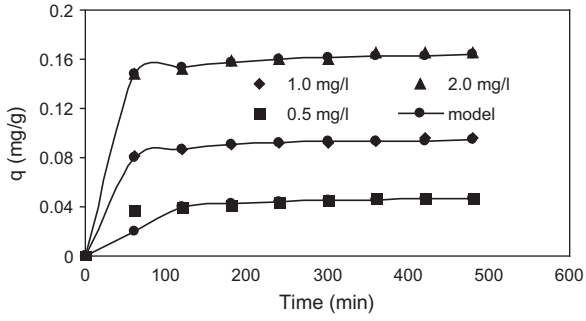

Fig. 12. Fitting of reaction rate model for As(III) adsorption onto DMICS at different initial As(III) concentrations.

pseudo-second-order model is better fitted when compared with reaction rate model. The pseudo-second-order kinetic model is well suited to present experimental data. In accordance with the pseudo-second-order reaction mechanism, the overall rate of As(III) sorption appears to be controlled by the chemical processes i.e. it relies on the assumption that chemisorption may be the rate-limiting step. In chemisorption, the metal ions stick to the adsorbent surface by forming a chemical (usually covalent) bond and tend to find sites that maximize their coordination number with the surface [40].

Post pH of the solutions was measured after each experiments and it was observed that pH drift for 0.5 mg/L initial concentration ranged from 7.42 to 7.60. With the increase in initial concentration from 0.5 mg/L to 1.0 mg/L, the measured post pH of the solution ranged from 6.77 to 6.95. Further increase in the initial concentration up to 2.0 mg/L, the observed increase in post pH of the solution was from 7.27–7.52 (Table 6).

In order to assess the nature of the diffusion process responsible for adsorption of As(III) on DMICS, attempts were also made to calculate the coefficients of the process. Assuming spherical geometry for the sorbent, the overall rate constant of the process can be correlated with the pore diffusion coefficient (D_p) and film diffusion (D_f) coefficient independently in accordance with the following expressions [38]:

$$D_f = 0.23\frac{r_0 \delta C_0}{t_{1/2}} \quad (12)$$

$$D_p = 0.03\frac{r_0^2}{t_{1/2}} \quad (13)$$

where r_0 is the radius of the adsorbent (0.023 cm), δ is the film thickness (assumed as 10^{-3} cm) and C_0 is the initial concentration in mg/L.

Song et al. [41] suggested a relationship between $t_{1/2}$ and K_2 to obtain $t_{1/2}$ values as:

$$t_{1/2} = \frac{1}{K_2 q_e} \quad (14)$$

Employing the appropriate data and the respective overall rate constants, pore and film diffusion coefficients for various concentrations of As(III) were calculated for the DMICS. The film diffusion process appears to be one of the main rate-limiting steps since the coefficient values are in the range of 10^{-6} – 10^{-8} cm^2/s.

3.6. Column experiment

The column experiments were performed at different bed depths at a fixed flow rate. The pH and initial concentration of As(III) was kept constant during this study. Initially, the adsorption was very rapid; it may be due to the availability of more reaction sites which were able to capture arsenic around the media. Due to the gradual occupancy of these sites, the uptake becomes less effective in the next stage of the process. The breakthrough curve became flatter with an increase in time for various media depths. Breakthrough curves between C/C_0 against time are shown in the Fig. 13. The breakthrough times for 20, 40, and 60 cms depths column were calculated as 24, 66, and 114 h, respectively.

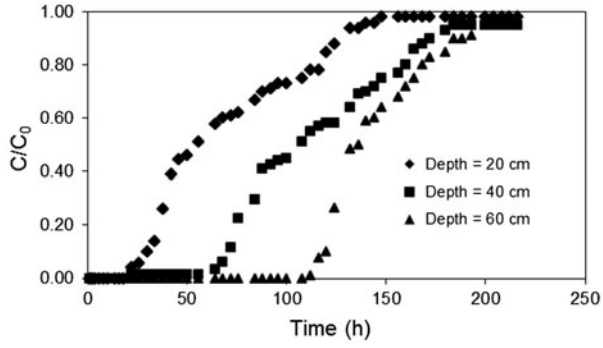

Fig. 13. Breakthrough curves of As(III) at different bed depths.

3.7. Spent media disposal

The spent adsorbents should fulfil the environmental regulations for use in landfill disposal. Toxicity leaching procedure test were designed to predict whether the contained pollutants like arsenic are likely to be hazardous for the surrounding environment or it is safe for disposal. When the leachate contains lower than 5 mg/L of arsenic, then the waste is identified as non-hazardous under US federal regulations and can be legally disposed as landfill. Concerning the leaching of arsenic, spent media have arsenic concentration of 60 μg/L. It was proved to be non-hazardous according to TCLP test.

3.8. Possible reaction mechanism

Arsenic removal by DMICS is governed by precipitation of iron on the surface of media. As(III) may be converted to As(V) in the presence of ferric (Fe^{+3}) ion on the DMICS surface [42].

$$As(III) + 2Fe(III) \rightarrow 2Fe(II) + As(V) \quad (15)$$

Oxidation of Fe(II) releases reactive oxidants, which can further oxidize As(III) species to more strongly adsorbable As(V) species. As(V) and—to a lesser extent—As(III) then adsorb to the coated sand particles where arsenic remains immobilized under oxic condition. After the conversion of As(III) to As(V), following reactions may take place on the DMICS surface [43].

$$SOH + H_3AsO_4 \leftrightarrow SH_2AsO_4 + H_2O \quad (16)$$

$$SOH + H_3AsO_4 \leftrightarrow SHAsO_4^- + H_2O + H^+ \quad (17)$$

where S stands for surface functional group.

Some of the As that remains in the form of As(III) following reactions may be possible on the DMICS surface [6].

$$M - FeOH + H_3AsO_3 \rightarrow M - Fe - H_2AsO_3 \quad (18)$$

where M stands for media.

4. Conclusions

In this study, an extensive laboratory investigations were carried out to evaluate the As(III) adsorption capacity of laboratory-developed adsorbent media (DMICS). The images of SEM of arsenic-loaded DMICS show uneven and chapped-like surfaces. The XRD of plain sand, DMICS and arsenic-loaded DMICS show various peaks of iron-based salts. Langmuir isotherm is better fitted with the experimental data when compared with other isotherms tried for this study. Based on batch kinetic model studies, pseudo-second-order model has shown better correlation. This correlation shows chemisorption may be predominant sorption mechanism. The DMICS is effective filter material for the treatment of arsenic-contaminated water during column studies. DMICS has shown a good potential for environmental remediation of arsenic-contaminated groundwater.

Nomenclature

A	—	Temkin constant, (L/g)
B	—	Temkin constant, (mg/g)
b	—	parameter of Langmuir equation, (L/mg) a constant related to energy and enthalpy of the system
C	—	liquid-phase As(III) concentration at time t, (mg/L)
C_e	—	liquid-phase As(III) concentration at equilibrium, (mg/L)
C_0	—	initial As(III) concentration in the aqueous phase, (mg/L)
d_p	—	geometric mean size diameter of particle, (mm)
D_f	—	film diffusion coefficient, (cm^2/s)
D_p	—	pore diffusion coefficient, (cm^2/s)
K_2	—	rate constant of second-order rate model, (g/mg·min)
K_F	—	parameter of Freundlich equation, (mg/g)
K_R	—	rate constant of reaction rate model, (L/mg·h)
K_s	—	dimensionless constant separation factor
m	—	dose of DMICS, (g/L)
n	—	constant of Freundlich equation
N	—	number of measurements
q	—	amount of As(III) adsorbed at time t, (mg/g)
q_e	—	amount of As(III) adsorbed at equilibrium, (mg/g)
q_{exp}	—	experimental value of As(III) adsorbed at certain time t, (mg/g)
q_{mod}	—	model-simulated value of As(III) adsorbed at time t, (mg/g)
Q_o	—	sorption capacity of media as per Langmuir isotherm, (mg/g)
r_0	—	radius of the adsorbent, (cm)
RMSE	—	root mean square error
R^2	—	correlation coefficient
δ	—	film thickness, (cm)

References

[1] C.K. Jain, I. Ali, Arsenic: Occurrence, toxicity and speciation techniques, Water Res. 8 (2000) 4304–4312.
[2] P.L. Smedley, D.G. Kinniburgh, A review of the source, behavior and distribution of arsenic in natural waters, Appl. Geochem. 17 (2002) 517–568.
[3] P. Mondal, C.B. Majumder, B. Mohanty, Laboratory based approaches for arsenic remediation from contaminated water: Recent developments, J. Hazard. Mater. B 137 (2006) 464–479.
[4] WHO, Guidelines for Drinking Water Quality, Recommendations, World Health Organization, Geneva, 2003.
[5] BIS, Drinking Water Standards (IS 10500-91), Beuro of Indian Standard, India, 2003.
[6] I.A. Katsoyiannis, A.I. Zouboulis, Removal of arsenic from contaminated water sources by sorption onto iron-oxide-coated polymeric materials, Water Res. 36 (2002) 5141–5155.
[7] T. Yoshida, H. Yamanchi, G.F. Jun, Chronic health effect in people exposed to arsenic via the drinking water: Dose-response relationship in review, Toxicol. Appl. Pharmacol. 198 (2004) 243–252.
[8] C.M. Su, R.W. Puls, Arsenate and arsenite sorption on magnetite: Relations to groundwater arsenic treatment using zerovalent iron and natural attenuation, Water Air Soil Pollut. 193 (2008) 65–78.
[9] V. Campos, P.M. Buchler, Anionic sorption onto modified natural zeolites using chemical activation, Environ Geol. 52 (2007) 1187–1192.
[10] P.M. Solozhenkin, A.I. Zouboulis, I.A. Katsoyiannis, Removal of arsenic compounds by chemisorption filtration, J. Min. Sci. 43 (2007) 212–220.
[11] E.H. Smith, Modeling batch kinetics of cadmium removal by a recycled iron adsorbent, Sep. Sci. Technol. 33 (1998) 149–168.
[12] S. Oremland, J.F. Stolz, Ecology of arsenic, Science 300 (2003) 939–944.
[13] T.V. Nguyen, S. Vigneswaran, H.H. Ngo, J. Kandasamy, H.C. Choi, Arsenic removal by photo-catalysis hybrid system, Sep. Purif. Technol. 61 (2008) 44–50.

[14] M.G. Vaclavikova, S. Gallios, S. Hredzak, S. Jakabsky, Removal of arsenic from water streams: an overview of available technologies, Clean Technol. Environ. Policy, 10 (2007).
[15] M. Badruzzaman, P. Westerhoff, D. Knappe, Intraparticle diffusion and adsorption of arsenate onto granular ferric hydroxide (GFH), Water Res. 38 (2004) 4002–4012.
[16] R.C. Vaishya, S.K. Gupta, Coated sand filtration: An emerging technology for water treatment, J. Water Supply: Res. Technol.-AQUA 52 (2003) 299–306.
[17] R.C. Vaishya, S.K. Gupta, Optimization of oxide coating process on quartz sand for arsenic (III) removal from groundwater, J. Water Supply Res. Technol. Aqua 60 (2011) 109–120.
[18] A. Joshi, M. Chaudhuri, Removal of arsenic from ground water by iron oxide coated sand, J. Environ. Eng. 122 (1996) 769–771.
[19] O.S. Thirunavukkarasu, T. Viraraghavan, K.S. Subramanian, Arsenic removal from drinking water using iron-oxide coated sand, Water Air Soil Pollut. 142 (2003) 95–111.
[20] Eaton, Analytical Chemistry of As- Final Report, Vol. 914 , AWWARF, Denver, CO, 1996.
[21] Y.S. Han, T.J. Gallegos, A.H. Demond, K.F. Hayes, FeS-coated sand for removal of Arsenic (III) under anaerobic conditions in permeable reactive barriers, Water Res. 45 (2011) 593–604.
[22] H. Guo, D. Stüben, Z. Berner, Arsenic removal from water using natural iron mineral–quartz sand columns, Sci. Total Environ. 377 (2007) 142–151.
[23] D.L. Johnson, M.E.Q. Pilson, Spectrophotometric determination of arsenite, ansenate and phosphate in natural waters, Anal. Chem. Acta 58 (1972) 289–299.
[24] S.L. Lo, H.T. Jeng, C.H. Lai, Characteristics and adsorption properties of iron-coated sand, Water Sci. Technol. 35 (1997) 63–70.
[25] J.A. Wilke, J.G. Hering, Adsorption of arsenic onto hydrous ferric oxide: Effects of adsorbate/adsorbent ratios and co-occurring solutes, Colloids Surf. A 107 (1996) 97–110.
[26] D.B. Singh, G. Prasad, D.C. Rupainwar, V.N. Singh, As(III) removal from aqueous solution by adsorption, Water Air Soil Pollut. 42 (1988) 373–386.
[27] L. Zeng, Arsenic adsorption from aqueous solutions on an Fe(III)-Si Binary Oxide Adsorbent, Water quality Res. J. Canada 39 (2004) 267–275.
[28] Langmuir, The constitution and fundamental properties of solids and liquids, J. Am. Chem. Soc. 38 (1916) 2221–2295.
[29] N. Ata, A. Olgun, Removal of basic and acid dyes from aqueous solutions by a waste containing boron impurity, Desalination 249 (2009) 109–115.
[30] W. Zhang, P. Singh, E. Paling, S. Delides, Arsenic removal from contaminated water by natural iron ores, Mineral Eng. 17 (2004) 517–524.
[31] T.A. Davis, B. Volesky, A. Mucci, A review of the biochemistry of heavy metal biosorption by brown algae, Water Res. 37 (2003) 4311–4330.
[32] B. Buchter, B. Davidoff, C. Amacher, C. Hinz, I.K. Iskandar, H.M. Selim, Correlation of Freundlich Kd and retention parameters with soils and elements, Soil Sci. 148 (1989) 370–379.
[33] R.M. Cornell, U. Schwertmann, The Iron Oxides, Structure, Properties, Reactions, Occurrence and Uses, VCH, Weinheim, 1996.
[34] M. Hodi, K. Polyak, J. Hlavay, Removal of pollutants for drinking water by combined ion-exchange and adsorption methods, Environ. Int. 21 (1995) 325–331.
[35] R.C. Vaishya, S.K. Gupta, Modeling arsenic(III) adsorption from water by sulfate modified iron-oxide coated sand (SMIOCS), Sep. Sci. Technol. 39 (2004) 645–666.
[36] T.S. Singh, K.K. Pant, Equilibrium kinetics and thermodynamic study for adsorption of As(III) on activated alumina, Sep. Purif. Technol. 36 (2004) 139–147.
[37] O.S. Thirunavukkarasu, T. Viraraghavan, K.S. Subramanian, O. Chaalal, M.R. Islam, Arsenic removal in drinking water-impacts and novel removal technologies, Energy Sources 27 (2005) 209–219.
[38] S.K. Maji, A. Pal, T. Pal, Arsenic removal from real-life groundwater by adsorption on laterite soil, J. Hazard. Mater. 151 (2008) 811–820.
[39] G.M. Hernandez, S. Rihs, A simplified method to estimate kinetic and thermodynamic parameters on the solid-liquid separation of pollutants, J. Colloid Interface Sci. 299 (2006) 49–55.
[40] P.W. Atkins, Physical Chemistry, 5th ed., Oxford University Press, Oxford, 1995.
[41] J. Song, W. Zou, Y. Bian, F. Su, R. Han, Adsorption characteristics of methylene blue by peanut husk in batch and column modes, Desalination 265 (2011) 119–125.
[42] M. Edward, Chemistry of arsenic removal during coagulation and Fe-Mn oxidation, J. Am. Water Works Assoc. 86 (1994) 64–79.
[43] A. Deliyanni, E.N. Peleka, K.A. Matis, Modeling the sorption of metal ions from aqueous solution by iron-based adsorbents, J. Hazard. Mater. 172 (2009) 550–558.